INVESTIGATING THE RELATIONSHIP BETWEEN WATER VAPOR CONVERGENCE AND SEVERE CONVECTION USING THE WRF MODEL AT 1KM RESOLUTION

James M. Done[*] Xiang-Yu Huang[1], and Bill Kuo
National Center for Atmospheric Research, Boulder, CO
1. On leave from the Danish Meteorological Institute

1 INTRODUCTION

Severe convection is often preceded by low-level water vapor convergence (as discussed in Banacos and Schultz, 2005) . Observations of water vapor convergence can potentially increase the lead-time and knowledge of locations for nowcasting severe weather. In this study, we examine results of high-resolution numerical simulations of severe convection at 1-minute output interval to determine the relationship between low-level water vapor convergence and severe convection. Three cases are selected from the period of the the Bow-Echo and Mesoscale Convective Vortex Experiment (BAMEX), each of different convective-system mode; a bow-echo system, a leading-line Mesoscale Convective System (MCS) and a line of supercells. The Weather Research and Forecasting (WRF) model is used with one-way nesting to simulate the pre-convective environment, convection initiation and mesoscale organization at 1km horizontal grid-spacing.

Following Kuo (1974), low-level water vapor convergence is defined as;

$$-\int \rho \bigtriangledown . (q\mathbf{V}_h)dZ, \qquad (1)$$

where ρ is density, q is water vapor mixing ratio, $\mathbf{V}_h$ is the 2-dimensional wind field and Z is geopotential height. *Low-level* is defined here as the depth of the boundary layer of the convective environment taken from observed thermodynamic profiles.

Remote sensing methods often observe total colum water vapor, known as Precipitable Water (PW) and assume the time tendency of PW provides an estimate for low-level water vapor convergence. The time rate of change of total column water vapor can be expressed as;

$$\frac{\partial PW}{\partial t} = \int \rho Q \, dZ - \int \rho \bigtriangledown .\mathbf{V}q \, dZ + \int \rho q \bigtriangledown .\mathbf{V} \, dZ. \quad (2)$$

where $\mathbf{V}$ is the 3d wind field and Q represents the sources and sinks of water vapor mixing ratio. The time rate of change of PW therefore depends on the source/sink terms, the vertically integrated 3d water vapor convergence and a 3d mass convergence term. The time rate of change of PW and vertically integrated water vapor convergence are therefore not the same quantity, and they may have different relationships with severe convection.

2 METHODS

Selected Case Studies

Cases of severe convection are selected from the period of the the Bow-Echo and Mesoscale Convective Vortex Experiment (BAMEX; Davis *et al.* (2004)). The relationship between water vapor convergence and severe convection may depend on the convective environment and convective-system mode. Therefore, in an attempt to provide a set of cases representing a cross-section of convective environments, three cases are selected, each of different convective-system mode. Extensive observational data of the cases, including radar and satellite animations, are archived at $http : //www.joss.ucar.edu/bamex/catalog$.

Case 1 is a severe bow-echo system[1] observed during 9-10 June 2003. Two tornadic supercells formed over northeast Nebraska around 0000 UTC 10 June along and just ahead of an upper-level wave and associated surface cold front. Two distinct bow structures quickly developed and subsequently consolidated into a continuous line that assumed a storm motion of $17ms^{-1}$ towards the southeast ($128°$).

For case 2, convection initiated over Oklahoma and Kansas from 2100 UTC 10 June along a trailing cold front. Convection subsequently organized overnight into a leading-line MCS. Whereas the convective environment of case 1 was characterised by weak thermodynamic gradients at low levels, convection for this case was initiated along the strong thermodynamic gradient of the cold front.

Case 3 is a line of supercells that tracked across the Great Lakes region on 30th May 2003. An upper-level shortwave trough moved southeastward into the Great Lakes region, and convection was initiated under strong forcing along a trailing cold front south of a surface low. Although instability was weak to moderate, strong shear of the horizontal wind supported supercells.

[*]*Corresponding author address:* James M. Done, National Center for Atmospheric Research, P.O. Box 3000, Boulder, CO 80307, USA ; e-mail: done@ucar.edu

[1]See Fujita (1978) and Weisman (2001) for a description of bow-echo systems.

3 MODEL SETUP

BAMEX provided an unprecedented opportunity to evaluate many WRF model forecasts of severe convection. Done *et al.* (2004) showed explicit convection forecasts using WRF were able to accurately predict the number of MCSs daily, the convective-system mode and evolution of the MCSs.

The recently released Version 2.0.3 of the WRF model is used here with one-way nesting. All domains have 35 terrain-following levels specified in the vertical. The basic physics packages are the same for both domains and include the Mellor-Yamada-Janjic (ETA) boundary layer scheme, the Noah land surface model, and the Lin microphysics scheme with 6 prognostic moisture variables (derived from the original scheme described in Lin *et al.* (1983)). Second-order diffusion is applied in the horizontal, and damping is applied to vertical velocity. Convective parameterization is not used and no additional data are assimilated.

The parent domain used for all simulations is shown in Fig. 1 together with the 3 nested domains. The parent domain of 500 × 500 grid points uses 4km horizontal grid-spacing. A grid-spacing of 4km is considered sufficient to represent MCSs explicitly without the need for a parameterization of convection (Weisman *et al.*, 1997) but is still insufficient for representing many cell-scale processes critical for severe weather forecasting (as discussed in Bryan *et al.* (2003)). Initial and boundary conditions are derived from the 40km ETA analyses available at 3 hourly intervals. Nested domains of approximately 600 × 500 grid points use 1km horizontal grid-spacing, and are located such that convection initiates close to the center of the domain. Both parent and nested domains are initialized using the ETA analyses, approximately six hours prior to the observed initiation of convection. Data from the nested domain are archived every minute.

4 ANALYSIS OF CASE 1: BOW-ECHO SYSTEM, 9-10 JUNE 2003

The simulation of case 1 captured the initiation of convection close to the center of the nested domain at approximately 0130 UTC 10 June 2003. Model convection quickly organized into a propagating bow-echo system, as observed. Further convection initiated within the nested domain and subsequently merged with the bow-echo system. Figure 2 shows the evolution of the model bow echo system within the sub-region of the nested domain outlined in Fig. 1. This sub-region is used later to calculate area averaged quantities and to isolate the water vapor signature associated with the bow-echo system. The sub-region includes the pre-convective environment, initiation and organization of the bow-echo.

Relationship with Water Vapor Convergence
Figure 3a shows a timeseries of low-level water vapor convergence and 1 minute accumulated rainfall, averaged over the sub-region. 1-minute rainfall amount is used here as a proxy for convection. Water vapor convergence appears to evolve on two timescales; a slow increase in the hours before convection followed by a fast increase close to the onset of convection. This suggests mechanisms are operating on two timescales; the slow increase associated with the synoptic/mesoscale development of the convective environment and the fast increase associated with a precursor mechanism to convection. This suggests a relationship between low-level water vapor convergence and severe convection.

Figure 3b shows timeseries of the time rate of change of PW using $\triangle t$ = 1 minute and 1 minute accumulated rainfall, both averaged over the sub-region. As for low-level water vapor convergence, $\triangle PW/\triangle t$ evolves on two timescales; a slow increase on synoptic/mesoscale timescales in the hours before convecion followed by a fast increase close to the onset of severe convection. This suggests a relationship between $\triangle PW/\triangle t$ and severe convection.

Lead-Times of the Precursors to Severe Convection
Precursors to severe convection have been identified in the time-series of low-level water vapor convergence and $\triangle PW/\triangle t$. Knowledge of the lead-time of the precursor is useful for nowcasting purposes. An estimate for the lead-times can be obtained by correlating the 1-minute rainfall field with either the water vapor convergence field or the $\triangle PW/\triangle t$ field. Ratio Y is calculated as follows;

$$Y(t) = \frac{R(n)}{W(n-t)}, \qquad (3)$$

where R is the number of grid points exceeding a 1-minute rain amount threshold (R_c) at the time of the onset of severe convection n. For case 1, n = 560 minutes into the simulation. W is the number of those grid points that exceed a low-level water vapor convergence threshold (WV_c) at different lead times t. To obtain the ratio for $\triangle PW/\triangle t$, the low-level water vapor convergence field is substituted for the $\triangle PW/\triangle t$ field. In converting the fields to binary, dependence on the magnitude is removed, and the ratio becomes a measure of overlap between shapes in the rainfall and water vapor convergence or $\triangle PW/\triangle t$ fields.

Figure 4a shows the ratio Y as a function of lead-time, t, for different values of the tunable threshold parameters R_c and WV_c. The shape of the timeseries are not sensitive to the threshold parameters, and maximum ratios occur around 30 minutes lead-time for low-level water vapor convergence. Figure 4b shows the maximum ratios for $\triangle PW/\triangle t$ occur around 40 minutes.

Sensitivity to Averaging Area
A precursor to severe convection has been identified in low-level water vapor convergence on the scale of the sub-region averaging area (151km × 151km). For nowcasting purposes it is desirable to detect precursors over smaller spatial scales to be more precise on the location

for severe weather warnings. Here, the sensitivity of characteristics of the precursor to the averaging area are examined.

Figure 5 shows timeseries of area averaged low-level water vapor convergence and 1 minute accumulated rainfall for three averaging areas; 151km $\times$ 151km, 75km $\times$ 75km and 31km $\times$ 31km. The center grid-point for all averaging areas is the same. A precursor is present for all averaging area sizes, and the time of the peak magnitude in water vapor convergence has low sensitivity to the averaging area size. As the averaging area is reduced, the magnitude of the area-averaged quantities increases, since the center point lies approximately at the location of highest rainfall amount. Similar results are found for the precursor in $\triangle PW/\triangle t$ (not shown).

Sensitivity to Temporal and Spatial Resolution

To determine the repeat cycle and spatial resolution of low-level water vapor observations necessary to capture the precursor for nowcasting severe weather, the sensitivity of the precursor in low-level water vapor convergence to the spatial and temporal resolution of the data is examined.

Figure 6 shows there are no significant differences in the timeseries of area average water vapor convergence using different spatial and temporal resolution data for the range 1km - 30 km and 1 min to 30 min for an averaging area of 31km$\times$ 31km. Therefore, changes occur on timescales of 30 minutes or greater and spatial scales of 30km or greater, resulting in low sensitivity of the magnitude and 'shape' of the precursor. This result is independent of the averaging area size for square boxes with side lengths between 31km and 151km (not shown). Similar results are found for the precursor in $\triangle PW/\triangle t$ (not shown).

5 ANALYSES OF CASES 2 AND 3

Similar analysis as for case 1 has been performed for cases 2 and 3. Simulations of cases 2 and 3 both captured the approximate location and timing of convection initiation close to the center of the nested domains, and captured the observed convective mode; a leading line MCS for case 2 and a line of supercells for case 3.

As for case 1, simulations of cases 2 and 3 show fast increases in area averaged low-level water vapor convergence (shown in Fig. 7) and $\triangle PW/\triangle t$ (not shown) prior to severe convection. Again, these precursors suggest a relationship with severe convection. Using a similar correlation technique as for case 1, maximum correlations between the field of 1-minute rainfall and either water vapor convergence or $\triangle PW/\triangle t$ occur around lead-times of 20 minutes for case 2 and 30 minutes for case 3. In addition, characteristics of the precursors, such as the 'shape' and lead-time, have low sensitivity to the size of the averaging area (not shown), and to the spatial and temporal resolutions of the data in the range 1km - 30 km and 1 min - 30 min (not shown).

6 SUMMARY

High-resolution numerical simulations of severe convection have been examined using 1-minute output to determine the relationship between low-level water vapor convergence and severe convection.

For the range of convective situations, low-level water vapor convergence evolves on two timescales; a slow increase on synoptic/mesoscale timescales in the hours before convection followed by a fast increase close to the onset of severe convection. The rapid increase of water vapor (and its associated moisture convergence) can serve as a useful precursor to severe convection. Our results show a significant increase of water vapor convergence occurs prior to severe convection, with lead-times in the range of 20 to 40 minutes. This relationship appears to be quite robust for grid spacing smaller than 30km and temporal interval of 30 minutes or smaller, and compares well with an observational study (Seko *et al.*, 2004) that showed increases in water vapor 20 minutes prior to convective precipitation cores.

Based on these results, we conclude that observing instrumentation capable of providing a 10 min repeat cycle and at a resolution of 10km would be able to detect significant moisture convergence, and provide useful warning for the possibility of severe convection.

REFERENCES

Banacos, P. and Schultz, D. (2005). The use of moisture flux convergence in forecasting convective initiation: Historical and operational prespectives. *Wea. Forecasting.*, **20**, 351–366.

Bryan, G., Wyngaard, J., and Fritsch, J. (2003). Resolution requirements for the simulation of deep moist convection. *Mon. Wea. Rev.*, **131**, 2394–2416.

Davis, C., Atkins, N., Bartels, D., Bosart, L., Coniglio, M., Bryan, G., Cotton, W., Dowell, D., Jewett, B., Johns, R., Jorgenson, D., Knievel, J., Knupp, K., Lee, W.-C., McFarquar, G., Moore, J., Pryzbylinski, R., Rauber, R., Smull, B., Trapp, R., Trier, S., Wakimoto, R., Weisman, M., and Ziegler, C. (2004). The Bow-Echo and MCV Experiment (BAMEX): Observations and opportunities. *Bull. Amer. Meteor. Soc.*, **85**, 1075–1093.

Done, J., Davis, C., and Weisman, M. (2004). The next generation of NWP: Explicit forecasts of convection using the weather research and forecasting (WRF) model. *Atmos. Sci. Letters.*, **5**, 110–117.

Fujita, T. (1978). Manual of downburst identification for project NIMROD. In *Satellite and Mesometeorology Research Paper*, number 156, page 104 pp. Depart-

ment of Geophysical Sciences, University of Chicago.

Kuo, H.-L. (1974). Further studies of the parameterization of the influence of cumulus convection on the large-scale flow. *J. Atmos. Sci.*, **31**, 1231–1240.

Lin, Y.-L., Farley, R., and Orville, H. (1983). Bulk parameterisation of the snow field in a cloud model. *J. Clim. Appl. Meteorol.*, **22**, 1065–1092.

Seko, H., Nakamura, H., Shoji, Y., and Iwabuchi, T. (2004). The meso-gamma scale water vapor distribution associated with a thunderstorm calculated from a dense network of gps receivers. *J. Meteor. Soc. Japan.*, **82**, 569–586.

Weisman, M. (2001). Bow echoes: A tribute to T. T. Fujita. *Bull. Amer. Meteor. Soc.*, **82**, 97–116.

Weisman, M., Skamarock, W., and Klemp, J. (1997). The resolution dependence of explicitly modeled convective systems. *Mon. Wea. Rev.*, **125**, 527–548.
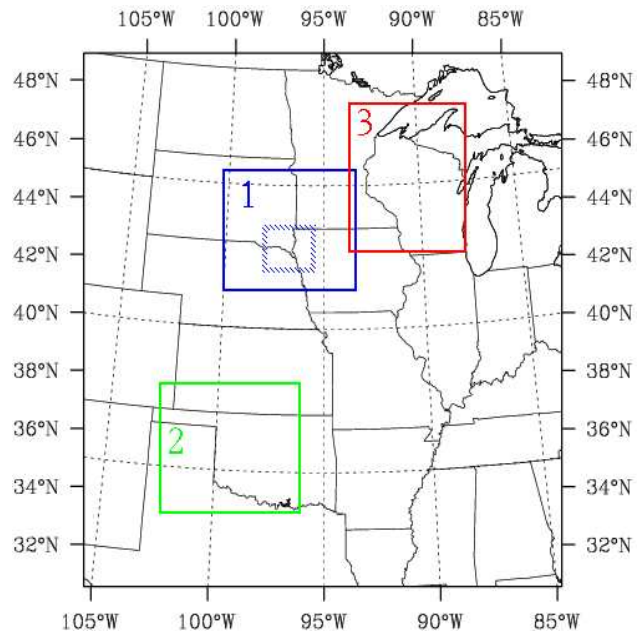
Figure 1: The parent domain (black) and nested domains for case 1 (blue), case 2 (green) and case 3 (red). Outlined in a blue dashed line is a sub-region of the nested domain for case 1 used to calculate area average quantities.

A 0145−0200 UTC
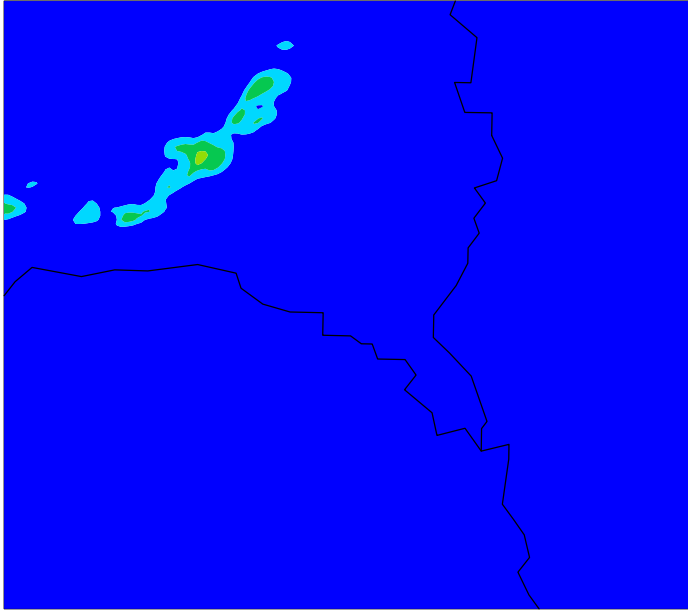
B 0245−0300 UTC
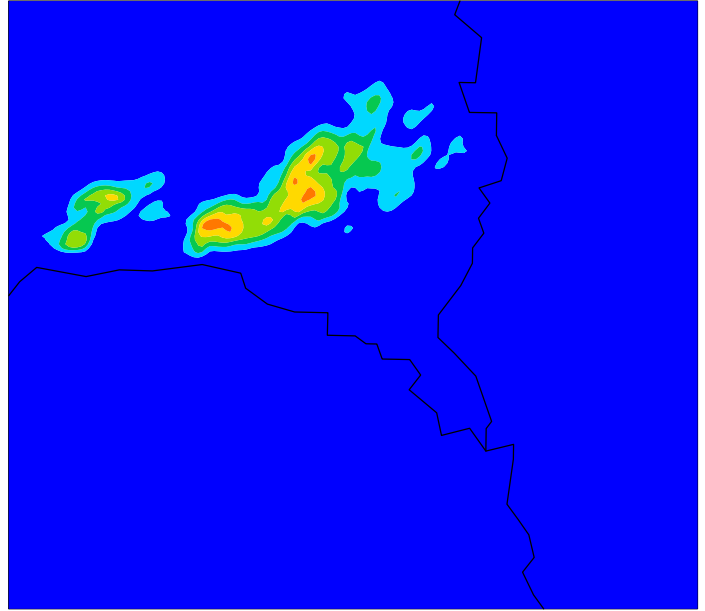
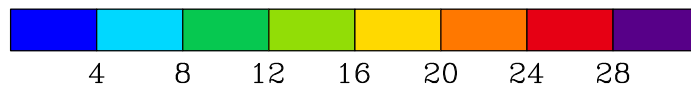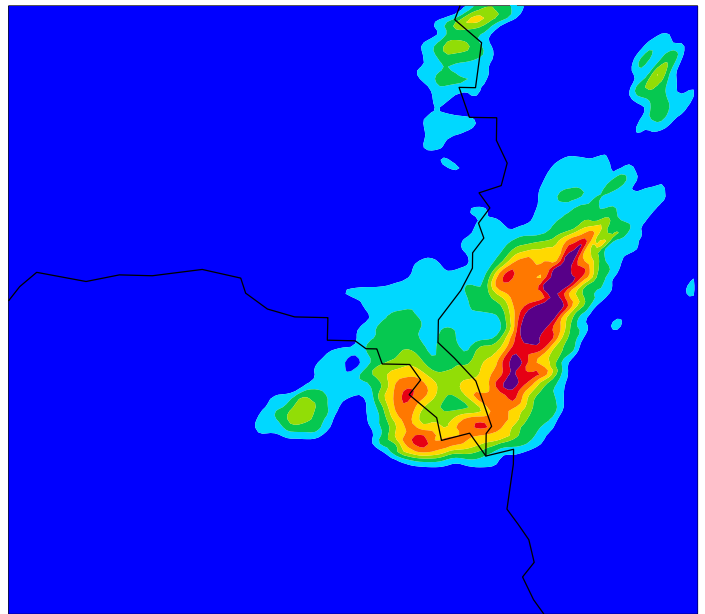C 0345−0400 UTC

D 0445−0500 UTC

4   8   12   16   20   24   28
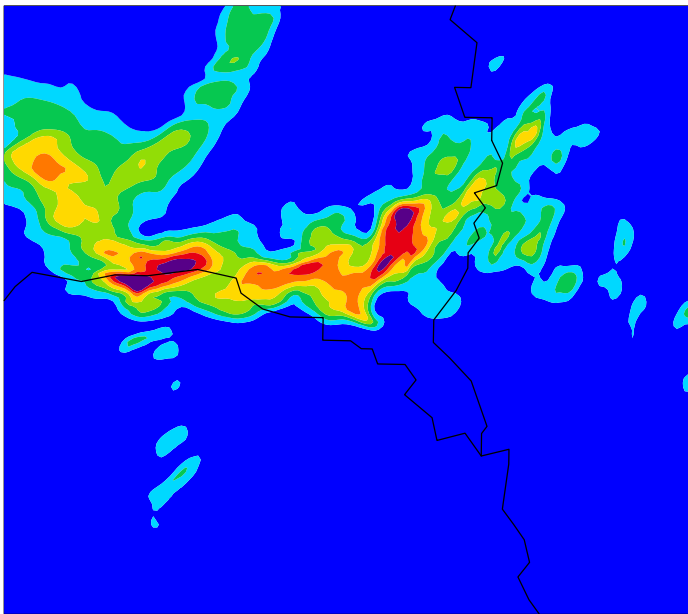
Figure 2: 15-minute accumulated rainfall (mm) shown for the sub-region of the nested domain for the periods (a) 0145-0200 UTC, (b) 0245-0300 UTC, (c) 0345-0400 UTC and (d) 0445-0500 UTC 10 June 2003.
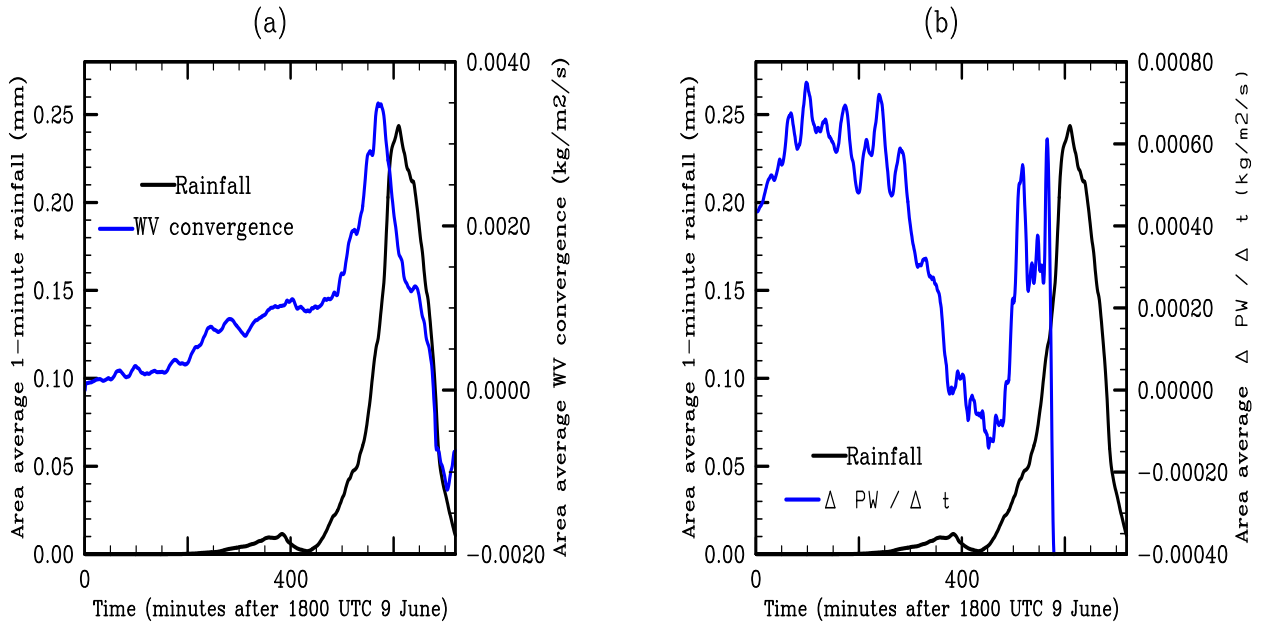
Figure 3: (a) Timeseries of 1-minute rainfall accumulation (mm, black) and low-level water vapor convergence (kgm^{-2}s^{-1}, blue), and (b) Timeseries of 1-minute rainfall accumulation (mm, black) and time rate of change of PW using $\triangle t$ = 1min (kgm^{-2}s^{-1}, blue). All quantities are area averages taken over the sub-region shown in Fig. 1.
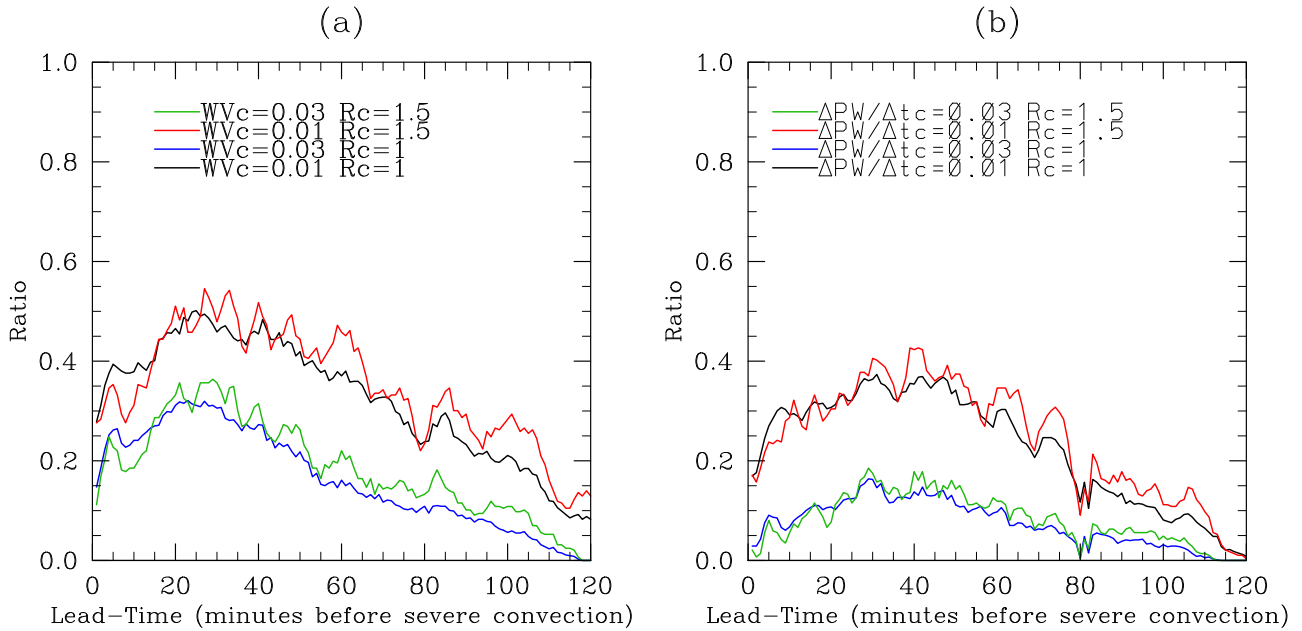
Figure 4: Ratio of the number of grid points exceeding a rainfall threshold to the number of those grid point exceeding (a) a water vapor convergence threshold and (b) a $\triangle PW/\triangle t$ threshold, for different thresholds.
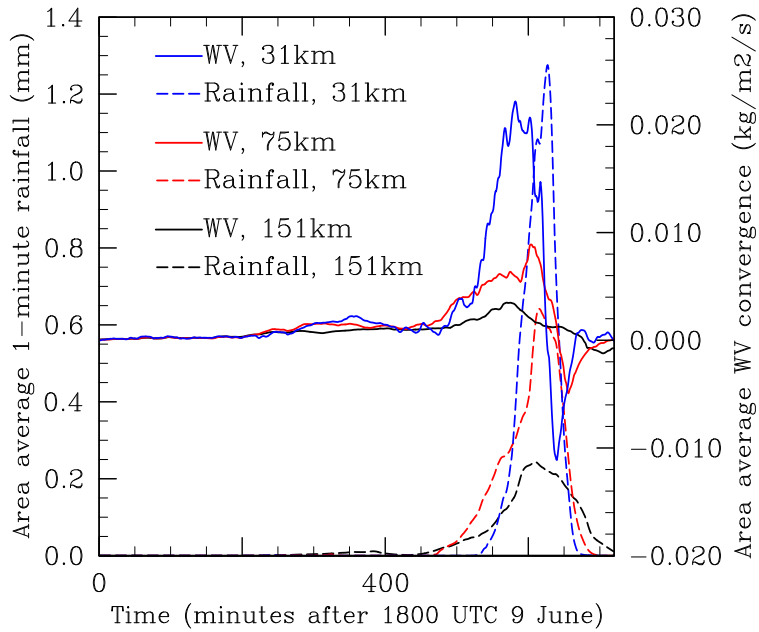
Figure 5: Timeseries of 1-minute rainfall accumulation (mm, dashed) and low-level water vapor convergence (kgm^{-2}s^{-1}, solid) averaged over square boxes of length 151km (black), 75km (red) and 31km (blue).

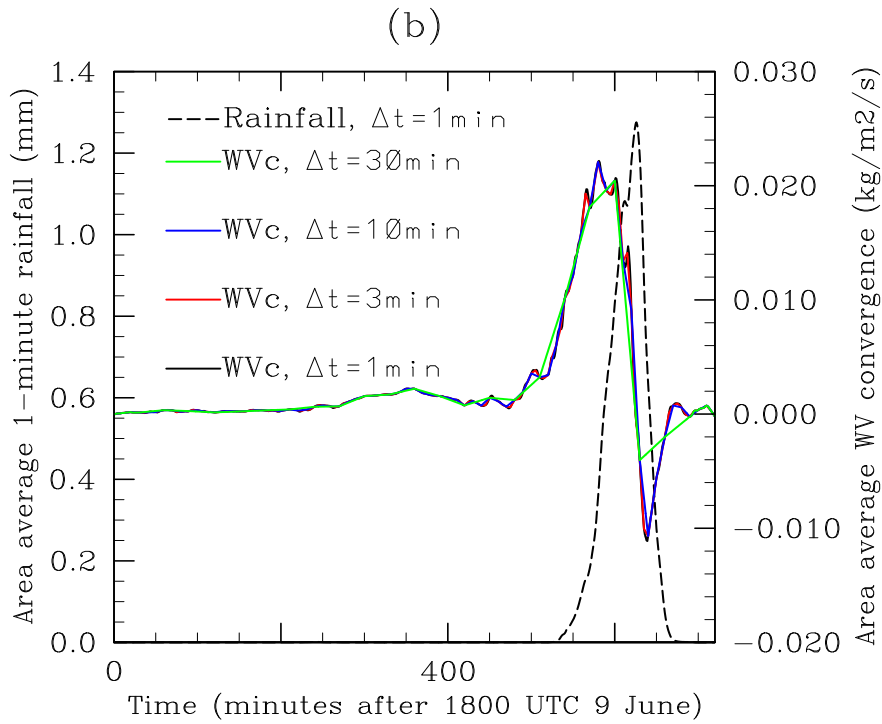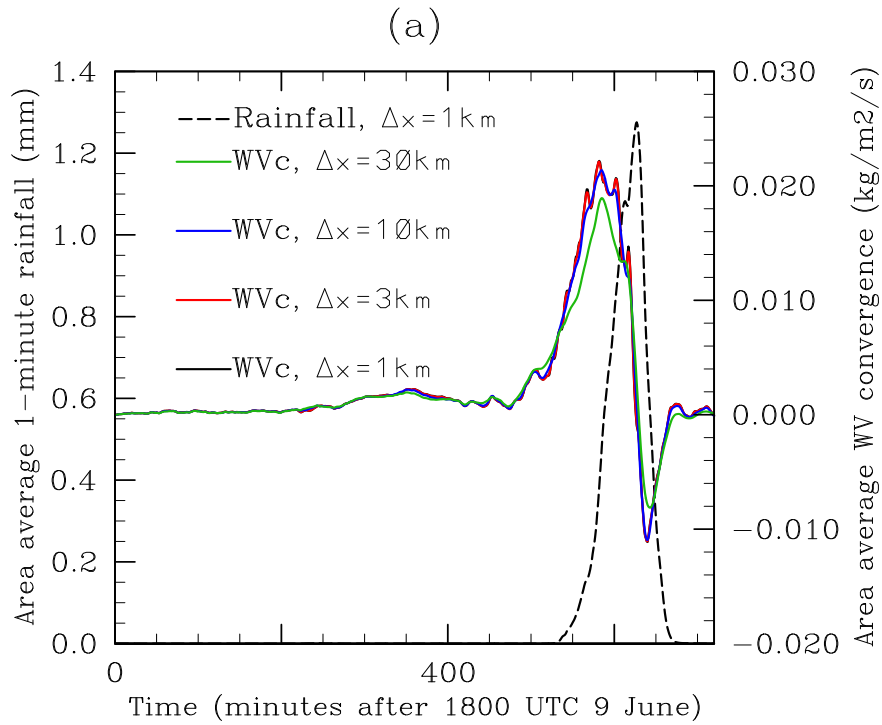Figure 6: Timeseries of 1-minute rainfall accumulation (mm, dashed) and low-level water vapor convergence (kgm^{-2}s^{-1}, solid) averaged over a 31km square box using (a) data of degraded spatial resolution and (b) data of degraded temporal resolution.
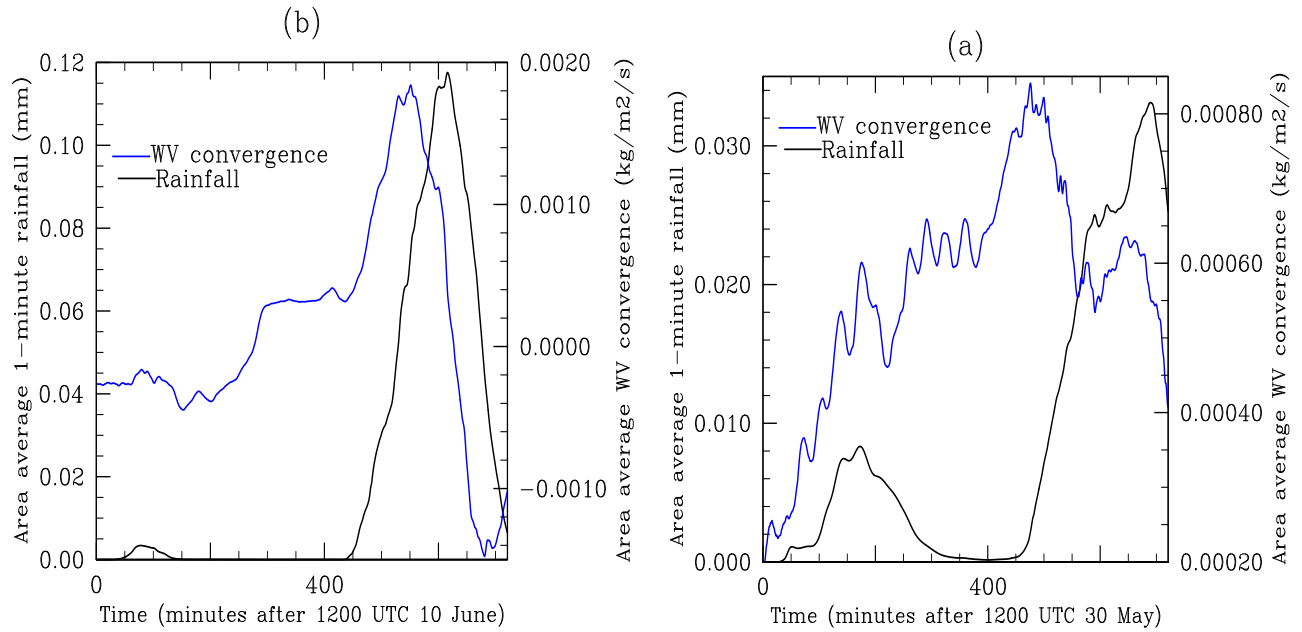
Figure 7: Timeseries of 1-minute rainfall accumulation (mm, black) and low-level water vapor convergence (kgm^{-2}s^{-1}, blue) averaged over a 151km square box for (a) case 2 and (b) case 3.